Advanced Journal of Chemistry, Section A

Journal homepage: www.ajchem-a.com

Original Research Article

Synthesis, IR and NMR–Spectroscopic, DFT Study of Aroyl Hydrazones 4,4,4-Trifluoro-1-(3-Furanyl)-1,3-Butanedione

Maftuna Jo'rayevna Ruzieva[1], Murod Amonovich Tursunov[1], Dana Sapargalievna Belgibayeva[2], Sardor Aminovich Karomatov[1], Bakhtiyor Shukurulloyevich Ganiev [1,*], Savriyeva Qahramon Qizi Nigina[3]

[1]*Department of Chemistry and Oil-Gas Technology, Bukhara State University, 200117, M. Ikbol Str., 11, Bukhara, Uzbekistan*
[2]*Department of Chemistry, L.N. Gumilyov Eurasian National University, Astana, Kazakhstan*
[3]*Bukhara State University, Bukhara, M. Ikbol Str., 11, 200117, Uzbekistan*

ARTICLEINFO

Article history

Submitted: 2025-10-05
Revised: 2025-11-28
Accepted: 2025-12-15
ID: AJCA-2510-1945
DOI: 10.48309/AJCA.2026.549860.1945

KEYWORDS

Hydrazone
DFT
HOMO
LUMO
Molecular docking

ABSTRACT

Aroyl hydrazones derived from 4,4,4-trifluoro-1-(3-furanyl)-1,3-butanedione represent a structurally distinctive and chemically significant class of organic compounds with considerable potential for application in various fields, including coordination chemistry, spectroscopy, and medicinal chemistry. These compounds exhibit versatile chelating behavior and are of great interest due to their pronounced biological activity. In the present study, a series of aroyl hydrazones was successfully synthesized via condensation of substituted acid hydrazides with the trifluoroacetyl moiety of the *β*-diketone precursor. Structural elucidation was carried out using Fourier-transform infrared (FTIR) spectroscopy, ^{1}H and ^{13}C nuclear magnetic resonance (NMR) techniques, and theoretical methods based on density functional theory (DFT). Experimental data correlated well with DFT-optimized structures, confirming the predominance of the hydrazone tautomer. Theoretical calculations also provided HOMO-LUMO energy levels, dipole moments, molecular electrostatic potential (MEP) maps, and Mulliken charge distributions. Molecular docking studies revealed energetically favorable binding interactions with *P. aeruginosa* target proteins. Molecular docking of the H_2L^1 ligand with the 1U1Z protein exhibited strong binding interactions (–11.6255 kcal/mol) via hydrogen bonds, π-π, and π-anion contacts, suggesting promising biological activity. Taken together, the findings of this study underline the potential applicability of these hydrazones as ligands for metal complexation and as promising bioactive compounds.

GRAPHICAL ABSTRACT

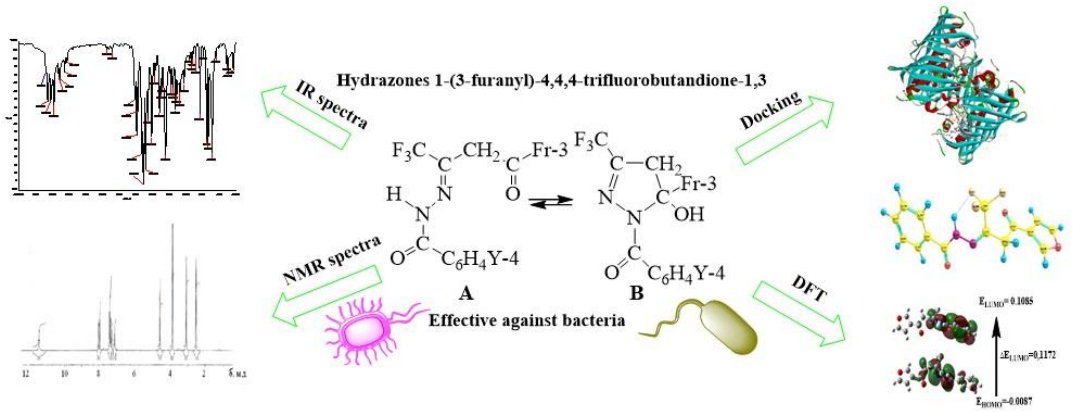

* Corresponding author: Ganiev, Bakhtiyor Shukurulloyevich
✉ E-mail: b.ganiyev1990@gmail.com

Introduction

Among the wide variety of organic ligands capable of complex formation, polydentate multifunctional ligands occupy a special place due to their ability to coordinate through multiple donor atoms, leading to highly stable and structurally diverse metal complexes [1-5]. The condensation reaction of fluorinated β-dicarbonyl compounds with acid hydrazides can proceed via both carbonyl groups. Since the β-dicarbonyl compound has a symmetric structure, the reaction results in the formation of positional isomers. Hydrazone derivatives have garnered considerable interest in contemporary organic and coordination chemistry due to their structural diversity, chelation ability, and extensive range of biological and pharmacological activities [4,6,7]. Among these, aroyl hydrazones represent a particularly versatile class of ligands capable of forming stable chelates with transition metal ions, which has prompted their exploration in fields such as catalysis, medicinal chemistry, and supramolecular design. The presence of donor atoms such as nitrogen and oxygen within the hydrazone framework facilitates their coordination to metal centers, enabling the formation of various geometrical and electronic configurations [5-10].

The condensation reaction between acid hydrazides and β-dicarbonyl compounds is a well-established method for synthesizing hydrazone compounds. In this context, the use of fluorinated β-diketones, such as 4,4,4-trifluoro-1-(3-furanyl)-1,3-butanedione introduces additional electronic features due to the highly electronegative trifluoromethyl group and the aromatic furanyl ring [9,11-14]. These structural motifs enhance the electron-withdrawing capacity of the hydrazone moiety, stabilizing specific tautomeric forms and potentially modulating their spectroscopic and electronic properties. Numerous studies have demonstrated the relevance of hydrazone-based compounds as antibacterial, antifungal, anticancer, and antioxidant agents [15-20]. The investigation of their structural behavior, tautomeric equilibrium, and bonding nature using experimental techniques like infrared (IR) and nuclear magnetic resonance (NMR) spectroscopy remains essential to understanding their physicochemical properties. Moreover, computational approaches such as density functional theory (DFT) have become indispensable tools in correlating theoretical predictions with experimental results. DFT calculations offer insights into molecular orbitals, charge distributions, dipole moments, and reactivity descriptors, supporting the rational design of hydrazone-based functional materials [20-22]. Aroyl hydrazones are versatile ligands that form complexes with various metal ions. Their biological activities, including antimicrobial, anticancer, and antioxidant properties, have been widely reported [15,16,20].

In this study, we report the synthesis of a series of aroyl hydrazones derived from 4,4,4-trifluoro-1-(3-furanyl)-1,3-butanedione and various substituted benzoyl hydrazides under mild conditions. The synthesized compounds were characterized using FTIR and ^{1}H-NMR spectroscopy, and their molecular structures were further investigated using DFT methods. A comprehensive analysis of tautomeric forms, HOMO-LUMO energy gaps, and molecular docking studies against *Pseudomonas aeruginosa* was conducted to evaluate their potential biological relevance. This integrated approach bridges synthetic organic chemistry and computational modeling to elucidate structure–activity relationships in novel hydrazone systems. Recently, a similar trifluoromethyl-containing 4,5-dihydro-1*H*-pyrazole derivative was synthesized and computationally analyzed [21].

Experimental

Materials and methods

All reagents, including 4,4,4-trifluoro-1-(3-furanyl)-1,3-butanedione (Sigma-Aldrich, Germany), substituted benzhydrazide (Sigma-Aldrich, Germany), and absolute ethanol (Medximfarmstroy, Uzbekistan), were obtained from commercial sources and used without further purification. Thin-layer chromatography (TLC) was performed on Silufol UV-254 plates (Merck, Germany). Deuterated solvents DMSO-d_6 and $CDCl_3$ (Merck, Germany) were employed for NMR spectroscopy. Prior to use, all solvents were carefully dried and distilled according to standard procedures. FTIR spectroscopic analysis was conducted using the infrared spectrometer "IR Tracer-100" Fure (Shimadzu, Japan), with wavelengths in the spectral range of 4,000-600 cm^{-1}, signal–to-noise sensitivity ratio of 60,000:1, scanning speed of 20 spectra per second. The ^{1}H-NMR spectra of the aroyl hydrazones 4,4,4-trifluoro-1-(3-furanyl)-1,3-butanedione were recorded at the JNM-ECZ600R spectrometer (JEOL, Japan), using DMSO-d_6 as the solvent. DFT calculations were performed using the Gaussian 09 software package, employing the B3LYP functional and 3-21++G(d,p) basis set [23-25]. The study of the biological activity of the benzoylhydrazone 4,4,4-trifluoro-1-(3-furanyl)-1,3-butanedione was conducted through molecular docking simulations using the Argus Lab software [26]. The active site of the proteins was defined within a grid size of 60×60×60 Å. The 3D structure of the *P. aeruginosa* (*Pseudomonas aeruginosa*) protein for this study (PDB ID: 1U1Z) was obtained from the Protein Data Bank. The results of the molecular docking were visualized using the Discover Studio Visualizer 4.0 software [27,28].

Synthesis of aroyl hydrazones

Aromatic acid hydrazides react with 4,4,4-trifluoro-1-(3-furanyl)-1,3-butanedione under mild conditions (ethanol as solvent, room temperature, no catalyst) via the trifluoroacetyl carbonyl group through a condensation reaction. The obtained product was purified by recrystallization from ethanol [29,30].

Synthesis of H_2L^1. To a solution of 2.06 g (0.01 mol) of 4,4,4-trifluoro-1-(3-furanyl)-1,3-butanedione in absolute ethanol, a solution of 1.36 g (0.01 mol) of benzoylhydrazine in absolute ethanol was added. The reaction mixture was maintained at 35–40 °C and monitored using thin-layer chromatography (TLC) on a Silufol UV-254 plate (eluent: $CHCl_3$). Upon completion of the reaction, the solvent was evaporated, yielding 2.6892 g (83%) of benzoylhydrazone of 4,4,4-trifluoro-1-(3-furanyl)-1,3-butanedione (H_2L^1).

The other derivatives of 4,4,4-trifluoro-1-(3-furanyl)-1,3-butanedione were synthesized under identical conditions (Table 1).

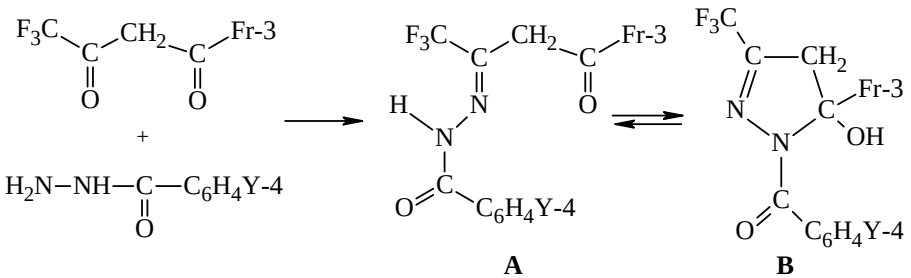

Y=H (H_2L^1); CH_3 (H_2L^2); OCH_3 (H_2L^3); Cl (H_2L^4); Br (H_2L^5); NO_2 (H_2L^6)

Scheme 1. Synthesis of the hydrazone derivative from aromatic acid hydrazides and 4,4,4-trifluoro-1-(3-furanyl)-1,3-butanedione under mild conditions (ethanol, room temperature, no catalyst)

Table 1. Reaction yield, melting point, and elemental analysis results of 4,4,4-trifluoro-1-(3-furanyl)-1,3-butanedione -aroylhydrazones

Compound	Yield, %	$T_{melt.}$, °C	Brutto-formula	Found/calculated, %			
				C	H	F	N
H_2L^1	83	132	$C_{15}H_{11}F_3N_2O_3$	55.51/55.56	3.36/3.39	17.55/17.59	8.67/8.64
H_2L^2	78	136	$C_{16}H_{13}F_3N_2O_3$	56.77/56.80	3.43/3.46	16.83/16.86	8.31/8.28
H_2L^3	82	143	$C_{16}H_{13}F_3N_2O_4$	54.39/54.24	3.65/3.67	16.06/16.10	7.95/7.91
H_2L^4	74	152	$C_{15}H_{10}F_3N_2O_3Cl$	50.18/50.21	2.76/2.79	15.85/15.90	7.85/7.81
H_2L^5	76	160	$C_{15}H_{10}F_3N_2O_3Br$	44.63/44.66	2.43/2.48	14.11/14.14	6.99/6.95
H_2L^6	85	156	$C_{15}H_{10}F_3N_3O_5$	48.75/48.78	2.67/2.71	15.42/15.45	11.43/11.38

Results and Discussion

IR spectroscopy

The IR spectra of the synthesized hydrazones exhibited distinct absorption bands corresponding to specific functional groups [31]. A prominent absorption band near 1,680 cm^{-1} was attributed to the C=O stretching vibration of the keto group, while bands around 1,600 cm^{-1} and 3,200–3,400 cm^{-1} were associated with the C=N and N-H stretching vibrations, respectively [14,32-34]. These spectral features confirm the successful condensation process and the formation of hydrazone linkages. The synthesized ligands are crystalline in nature and primarily exist in the hydrazone tautomeric form (a), as confirmed by IR spectral analysis of ligand H_2L^1 (Figures 1-3).

Within the spectral region corresponding to the vibrational frequencies of multiple bonds, several intense absorption bands were observed. Notably, no absorption bands were detected above 1,710 cm^{-1}, a characteristic feature of the N(S=O) stretching vibration associated with the CF_3 C=O fragment [9,10,32] (Figures 1-9). This observation indicates that the condensation reaction proceeded via the carbonyl group adjacent to the trifluoromethyl substituent. If the reaction had instead involved the alternative carbonyl group, the N(S=O) stretching vibration corresponding to the CF_3 moiety would have been observed within the 1,750–1,765 cm^{-1} range (Figure 10).

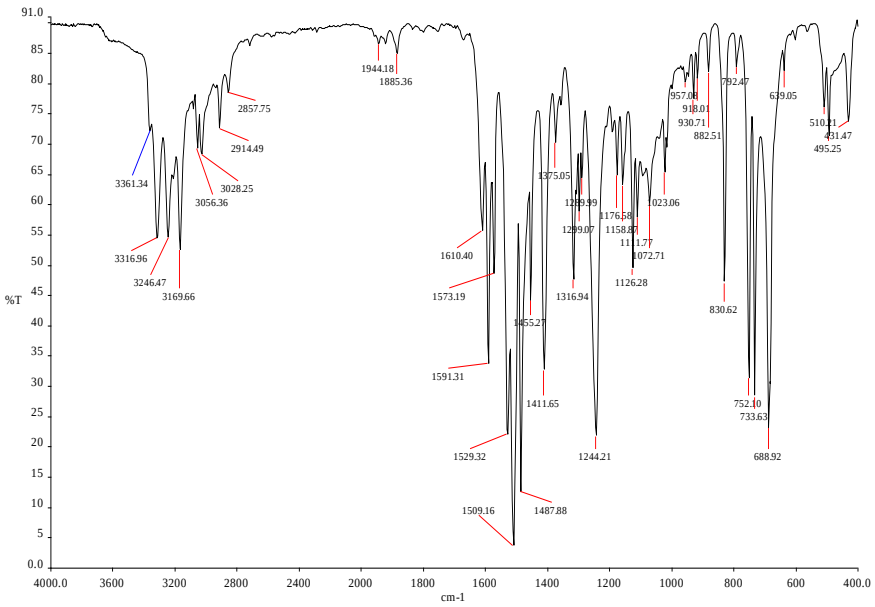

Figure 1. IR spectrum of H_2L^1

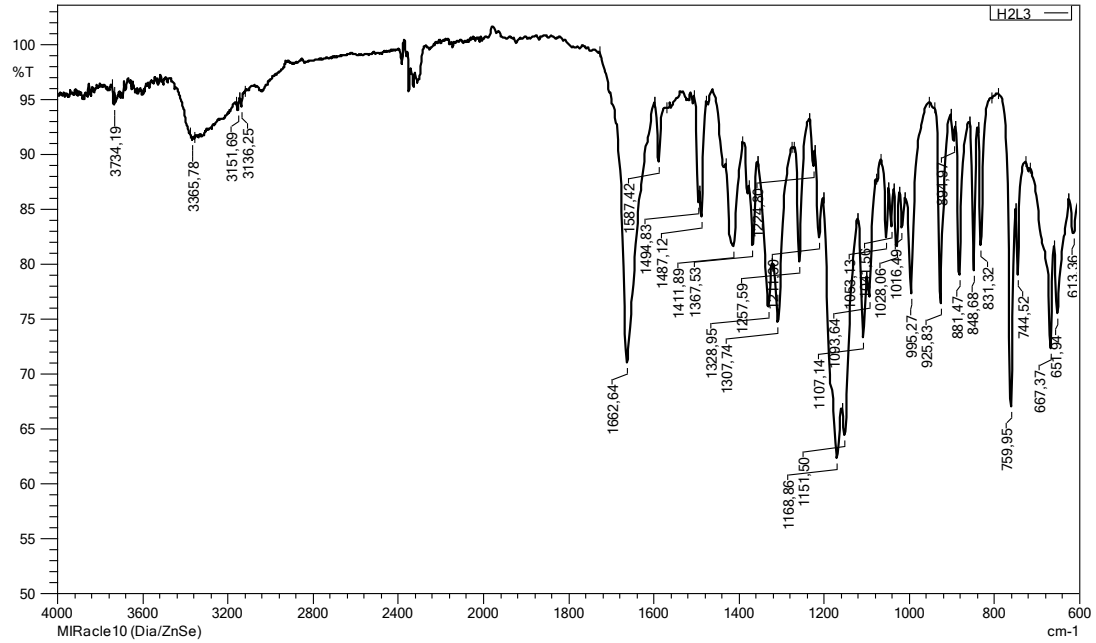

Figure 2. IR spectrum of H_2L^2

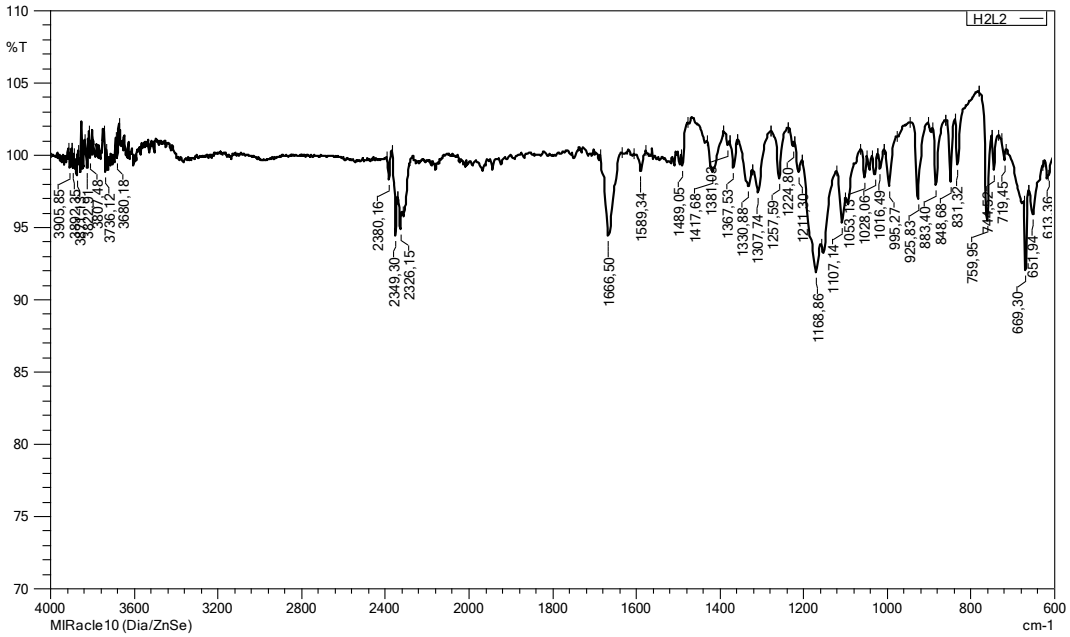

Figure 3. IR spectrum of H_2L^3

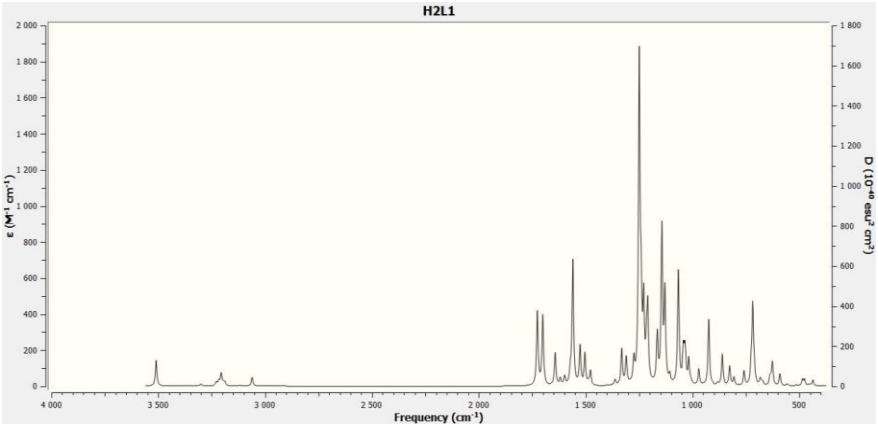

Figure 4. Theoretical calculated IR spectra of H_2L^1

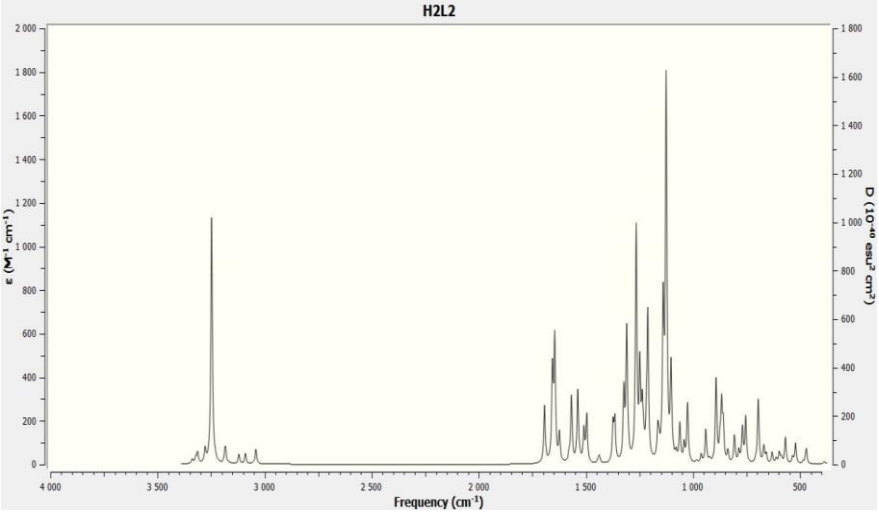

Figure 5. Theoretical calculated IR spectra of H_2L^2

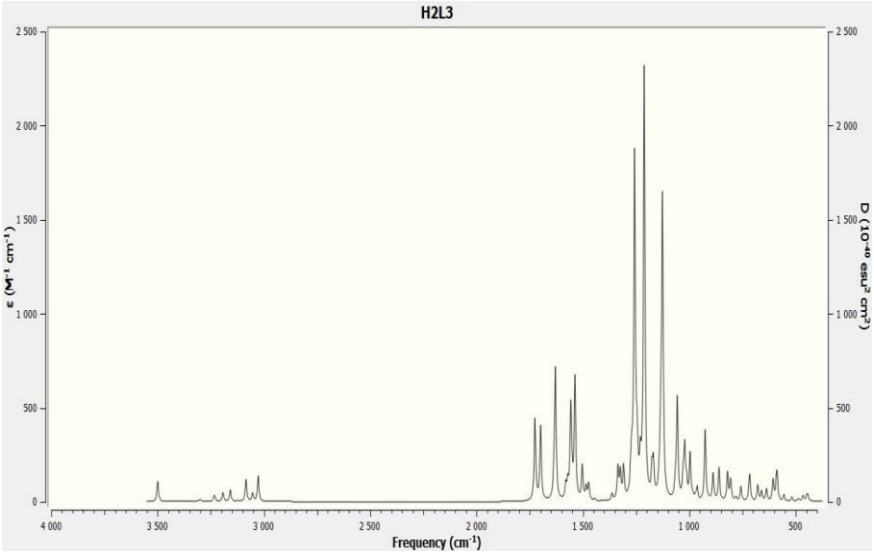

Figure 6. Theoretical calculated IR spectra of H_2L^3

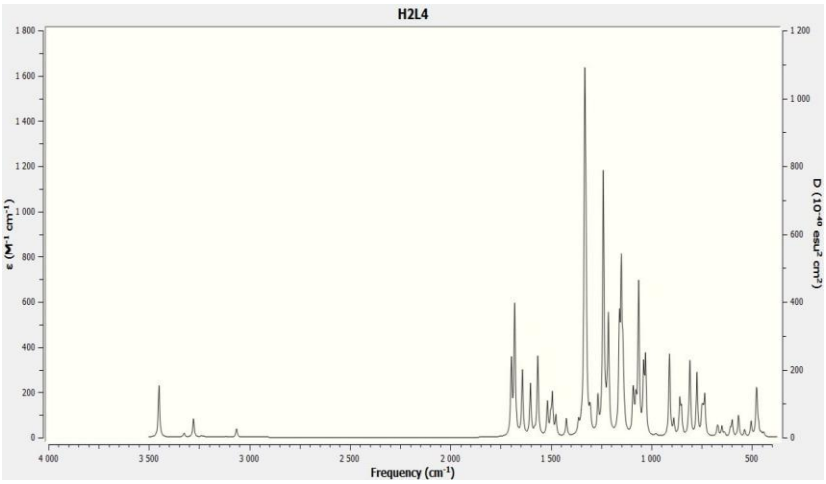

Figure 7. Theoretical calculated IR spectra of H_2L^4

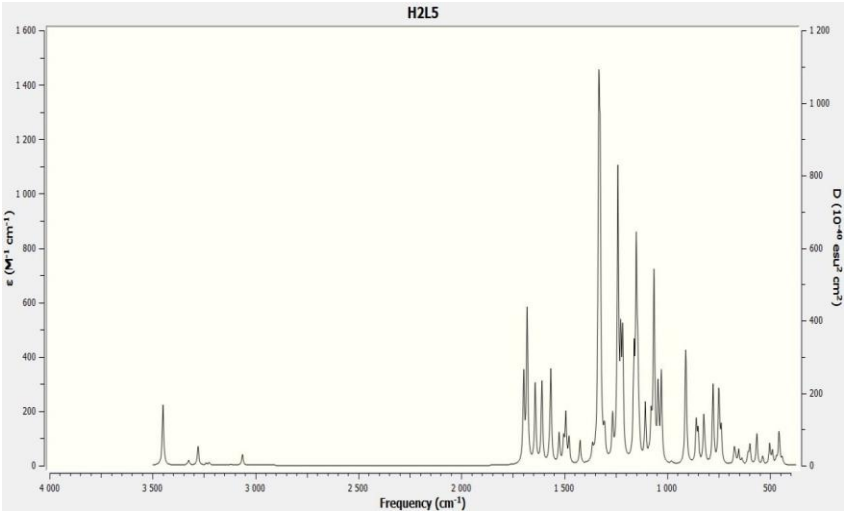

Figure 8. Theoretical calculated IR spectra of H_2L^5

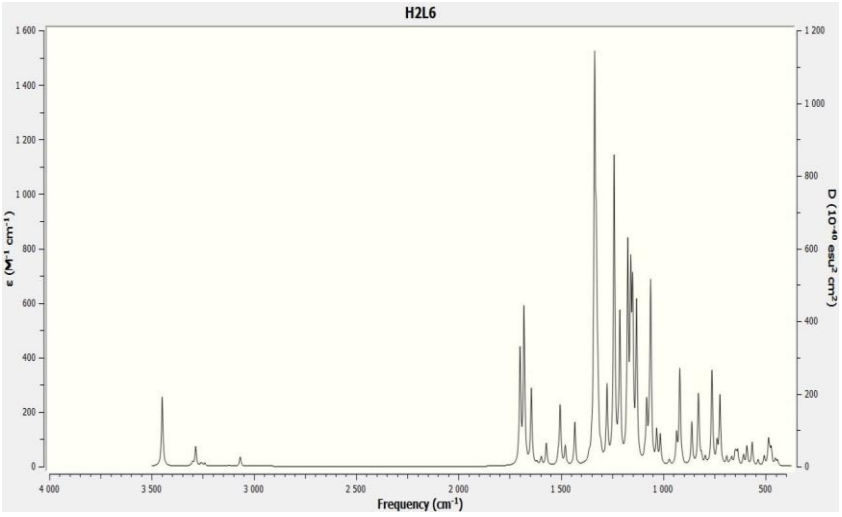

Figure 9. Theoretical calculated IR spectra of H_2L^6

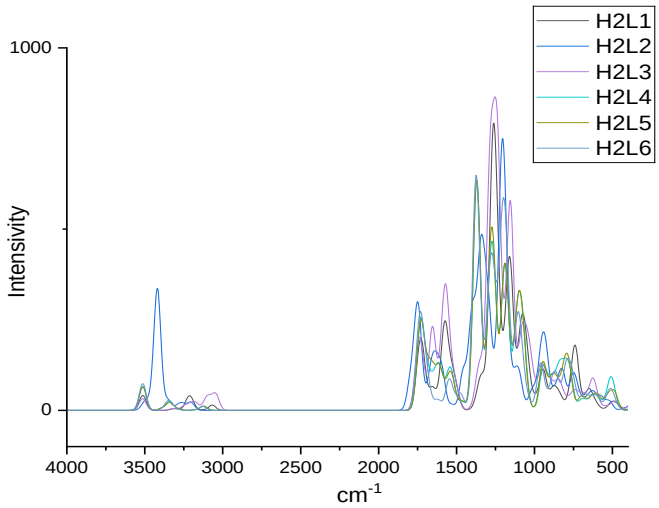

Figure 10. Compared theoretical IR spectra of H_2L^1, H_2L^2, H_2L^3, H_2L^4, H_2L^5, and H_2L^6

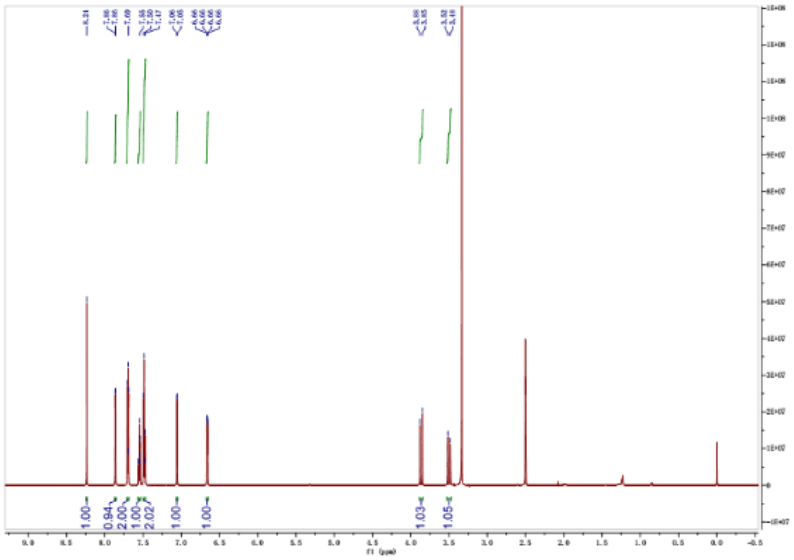

Figure 11. ^{1}H-NMR spectrum of 5-hydroxy-5-(furan-2-yl)-1-(4-methylphenyl)-3-(trifluoromethyl)-4,5-dihydro-1*H*-pyrazole-(H_2L^1) in DMSO-d_6 solution

NMR spectroscopy

The proton (^{1}H) and carbon (^{13}C) nuclear magnetic resonance (NMR) spectra provided confirmation of the structural composition of the synthesized compounds (Figures 11-13). Notable spectral signals included the imine proton (C=N), observed within the chemical shift range of δ 8.5–9.2 ppm, as well as aromatic proton signals corresponding to the furanyl and aroyl groups [35,36]. Additionally, the trifluoromethyl group exhibited a characteristic ^{11}F signal in the theoretical spectrum, appearing between δ -62 and -65 ppm, which highlights its electron-withdrawing effect on the hydrazone framework. NMR spectroscopic method has been used to study the tautomeric state of the synthesized ligands in solution. For example, when observing the NMR spectrum of the H_2L^2 ligand obtained in freshly prepared DMSO-d_6 (Figure 12), signals characteristic of the methyl group, α-methylene protons, and NH-group protons bound to the *β*-diketone part of the molecule have been observed in the region of δ 2.40; 4.50; and 11.45 m.h. with a

relative intensity of 3:2:1. The protons of the phenyl group have been observed as multiplet signals centered at δ 7.28; and 7.70 m.p., and the three protons of the furanyl fragment have been observed as doublets of equal intensity in the δ 7.26; 7.46; and 8.02 m.p. regions [32]. The signals corresponding to these protons have been partially obscured by those of the aromatic nucleus. The stability of the spectral profile over time suggests that the compound exclusively adopts the hydrazone (A) tautomeric form in this solvent, without undergoing interconversion into alternative tautomeric structures such as en-hydrazine or 5-hydroxy-2-pyrazoline (Figure 13 and Table 2).

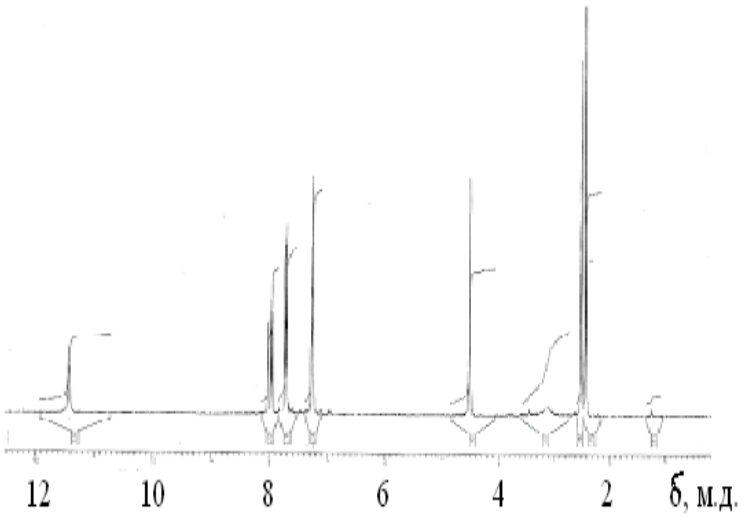

Figure 12. ^{1}H-NMR spectrum of 5-hydroxy-5-(furan-2-yl)-1-(4-methylphenyl)-3-(trifluoromethyl)-4,5-dihydro-1*H*-pyrazole - (H_2L^2) in DMSO-d_6 solution

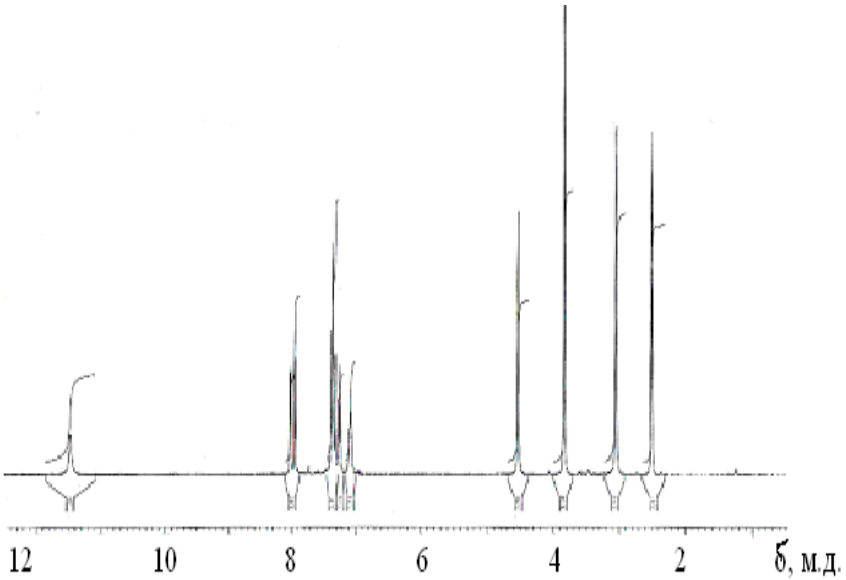

Figure 13. ^{1}H-NMR spectrum of 5-Hydroxy-5-(furan-2-yl)-1-(4-methoxybenzoyl)-3-(trifluoromethyl)-4,5-dihydro-1*H*-pyrazole (H_2L^3) in $CDCl_3$ solution

The NMR spectra of the condensation products of other aromatic acid hydrazides with 4,4,4-trifluoro-1-(3-furanyl)-1,3-butanedione (compounds H_2L^1, H_2L^3–H_2L^6) obtained in DMSO-d_6 solution are similar to the NMR spectrum of the H_2L^2 ligand, with the H_2L^1 and H_2L^3 compounds differing in the presence of signals from the protons of the substituents in the aromatic nucleus and the protons of the aromatic nucleus (Table 2). For example, while the methyl group of the H_2L^2 ligand is recorded in the d region of δ 2.40 m.p., in the ^{1}H-NMR spectrum of the H_2L^3 ligand, which is the condensation product of 4,4,4-trifluoro-1-(3-furanyl)-1,3-butanedione anisic acid with hydrazide (Figure 14), the protons of the CH_3O-group are recorded as a singlet signal in the δ region of 3.92 m.p. All this proves that the condensation product proceeds through the trifluoroacetyl carbonyl and exists in the hydrazone (A) form in solution, as in the crystalline state, and does not transform into other tautomeric forms in DMSO-d_6 solution (Table 3).

The conclusions drawn from the ^{1}H-NMR spectra are also confirmed by the results of the ^{13}C NMR spectrum obtained for the H_2L^3 ligand; the singlet signal of the carbon atom bound to the fifth member of the 5-hydroxy-2-pyrazoline ring resonates at δ 94.00 m.p. In addition, the presence of the hydrazone (A) tautomeric form is also confirmed by the signal of the carbon atom of the C=N bond at δ 135.08 m.p.

Importantly, the spectrum of this compound, like that of hexafluoroacetylacetone benzoyl-hydrazone, is characterized by a quartet splitting with a CTE of 33.9 Hz, which is observed only when adjacent to the CF_3-group. This indicator once again proves that the nucleophilic substitution reaction took place on the trifluoroacetyl carbonyl. The ^{1}H and ^{13}C NMR spectra of 4,4,4-trifluoro-1-(3-furanyl)-1,3-butanedione aroylhydrazones obtained in DMSO-d_6 solution do not change with time, indicating that in this solvent the organic substance hydrazone (A) is in the tautomeric form, and various tautomeric and configurational changes are not observed. Taking into account the size of the trifluoromethyl substituent, the hydrazone form is stabilized and exists mainly in the E-configurational form. For the Z-isomer, the internal strain in the molecule along the C=N bond is large, which is considered energetically unfavorable. If $CDCl_3$ is used as the solvent for spectrum acquisition, the shape and parameters of the ^{1}H-NMR spectrum change over time. If these compounds are found to be in the hydrazone (A) form in a freshly prepared solution, a second set of resonance signals appears after 2-3 minutes, indicating the formation of the cyclic (B) tautomeric form.

Table 2. ^{1}H-NMR spectrum parameters of 1-aroyl-3-trifluoromethyl-5-hydroxy-5-furanyl-2 pyrazolines in DMSO-d_6 solution (δ, m.p.)

Ligands	Y	CH_2	NH	C_6H_4–X	C_4H_3S	Y
H_2L^1	H	4.55	11.52	7.48; 7.78	7.26; 7.56; 7.96	–
H_2L^2	CH_3	4.50	11.45	7.28; 7.70	7.26; 7.46; 8.02	2.40
H_2L^3	OCH_3	4.52	11.45	7.56;7.77	7.28; 7.53; 8.00	3.92
H_2L^4	Cl	4.57	11.59	7.50; 7.80	7.28; 7.96; 8.06	–
H_2L^5	Br	4.58	11.55	7.48; 7.75	7.28; 7.88; 8.03	–
H_2L^6	NO_2	4.69	11.62	7.54; 7.86	7.28; 7.49; 8.04	–

Table 3. Parameters of the NMR spectrum (δ, ppm) and tautomeric composition of 4,4,4-trifluoro-1-(3-furanyl)-1,3-butanedione -acylhydrazones obtained in $CDCl_3$ solution

Compound	A^2		B^2		A^2,	B^2,
	CH_2	NH	CH_2*	OH	%	%
H_2L^1	4.55	11.52	3.38; 3.58	5.66	75	25
H_2L^2	4.50	11.45	3.38; 3.60	5.61	77	23
H_2L^3	4.52	11.45	3.39; 3.61	5.58	78	22
H_2L^4	4.57	11.59	3.39; 3.60	5.52	75	25
H_2L^5	4.58	11.55	3.43; 3.66	5.44	75	25
H_2L^6	4.69	11.62	3.46; 3.69	5.48	75	25

Explanation: * $-J_{AB}$ = 19-20 Hz

After a short time (30 minutes), a ring-line tautomeric equilibrium is established between the A and B tautomeric forms. The rapid appearance of tautomeric equilibrium in solution leaves no doubt that the crystalline product H_2L^1 is indeed the E-configurational structure of the hydrazone (A) tautomer, since the spatial proximity of the molecular fragments bound by the NH- and C=O bonds facilitates the process of intramolecular cyclization. Thus, the condensation reactions of *β*-dicarbonyl compounds such as 4,4,4-trifluoro-1-(3-furanyl)-1,3-butanedione with acylhydrazides proceed in a completely different direction than in the case of aroyltrifluoroacetylmethane. While at room temperature the first type of diketones proceeds through the carbonyl of the aroyl group, in furanyl derivatives this reaction proceeds through the trifluoroacetyl carbonyl. Such reactivity of 4,4,4-trifluoro-1-(3-furanyl)-1,3-butanedione is explained by the fact that the strong electron donor sulfur atom forms a bonding system with the neighboring carbonyl group, which reduces its reactivity during attack by nucleophilic particles.

DFT calculations

DFT calculations provided optimized geometries and vibrational frequencies that closely matched experimental IR data (Figures 4-10).

The electronic structure analysis revealed significant delocalization of electron density across the hydrazone framework. The HOMO-LUMO gap indicated moderate electronic stability (Table 4) [24].

The dipole moment (μ_D) in chemistry quantifies the separation of charges within a molecule. As a vector quantity, it has both magnitude and direction. It plays a crucial role in understanding the electrical distribution in polar covalent bonds and its impact on molecular polarization and chemical behavior [20,32,37-40]. A higher dipole moment enhances the effectiveness of metal surface absorption. Table 4 illustrates the polarization of each molecule, calculated using quantum chemical methods in three dimensions. In summary, a greater dipole moment significantly influences molecular polarity, intermolecular forces, solubility, chemical reactivity, and optical properties. DFT calculations showed that the values of the dipole moments of the ligands increase; Hhowever, partial deviations are observed in the hydrazones H_2L^2 and H_2L^3.

The global electrophilicity index measures a molecule's ability to accept electrons. Molecules with a high electrophilic values function as effective electrophiles, whereas those with low values behave as nucleophiles. Nucleophiles donate electron pairs to form new chemical bonds, while electrophiles possess an affinity for accepting electrons. Molecules with elevated electrophilicity demonstrate greater electron-attracting capability, which directly influences their reactivity and bond-forming ability [23,38,40].

Table 4. Dipole moments, frontier molecular orbitals, gap values, and descriptors for the optimized structure of complex H_2L^1 - H_2L^6

Parameter	H_2L^1	H_2L^2	H_2L^3	H_2L^4	H_2L^5	H_2L^6
μ_D (Debye)	1.9848	3.3604	3.3058	5.3358	5.3420	5.8731
E_{HOMO} (eV)	-0.0087	-0.0514	-0.3420	-1.1616	-1.1632	-0.1249
E_{LUMO} (eV)	0.1085	0.1213	0.1036	0.0413	0.0234	0.1023
$\Delta E_{LUMO-HOMO} = E_{LUMO} - E_{HOMO}$ (eV)	0.1172	0.1727	0.4456	1.2029	1.1866	0.2272
Ionization energy, $I = -E_{HOMO}$ (eV)	0.0087	0.0514	0.3420	1.1616	1.1632	0.1249
Electron affinity, $A = -E_{LUMO}$ (eV)	-0.1085	-0.1213	-0.1036	-0.0413	-0.0234	-0.0234
Electronegativity, $\chi = (I + A)/2$ (eV)	-0.0499	-0.03495	0.2384	1.1203	0.5699	0.05075
Chemical potential, $\mu = -\chi$ (eV)	0.0499	0.03495	-0.2384	-1.1203	-0.5699	-0.05075
Global chemical hardness, $\eta = (I - A)/2$ (eV)	0.0586	0.08635	0.2228	0.60145	0.5933	0.07415
Global chemical softness, $S = 1/(2\eta)$ (eV^{-1})	8.532	5.8	2.244	0.8313	0.8427	6.743
Global electrophilicity index, $\omega = \mu^2/(2\eta)$ (eV)	0.0212	0.007	0.1275	1.0433	0.2737	0.0173
$\Delta N_{max} = -\mu/\eta$	-0.851	-0.4047	1.07	1.8626	0.9605	0.6844
Total energy, kJ/mol	-5.2584	-5.4289	-5.7552	-7.2527	-16.4248	-6.1451

The most considerable electron acceptance (electron neutrophils) was investigated with H_2L^4 compounds (1.0433 eV) and nucleophiles (H_2L^2, 0.007 eV). H_2L^4 has a high electron affinity of 1.0433 eV and H_2L^2 is a nucleophile with an electron affinity of 0.007 eV. Highly reactive nucleophiles with large values exhibit strong interactions with electrophiles. Both nucleophilic and electrophilic characteristics significantly contribute to the optical properties, stability, and chemical reactivity of high-value molecules. A positive charge transfer value (ΔN_{max}: H_2L^3, 1.07; H_2L^4, 1.8626; H_2L^5, 0.9605; and H_2L^6, 0.6844) indicates that the molecule acts as an electron acceptor, while a negative value (ΔN_{max}: H_2L^1, -0.8521; H_2L^2, -0.4047) signifies that it donates electrons. These findings reveal that energy variation is directly correlated with molecular hardness, particularly under conditions of simultaneous electron donation and back-donation. Larger energy gaps in ligands contribute to their enhanced chemical stability and decreased chemical reactivity. Soft chemical compounds exhibit greater reactivity, as they more readily donate electrons compared to more complex chemical compounds. The H_2L^4 compound demonstrates the highest chemical molecular hardness (0.60145 eV), as indicated by its maximum energy gap. In contrast, the H_2L^1 compound the lowest chemical softness (8.300 eV), corresponding to its minimal band gap energy. The HOMO-LUMO diagrams for H_2L^1 – H_2L^6 molecules are presented in Figure 14, while their physicochemical properties are summarized in Table 4.

The B3LYP functional in conjunction with the 3-21G(d) basis set was employed to determine the energy levels of the highest occupied molecular orbital (HOMO) and the lowest unoccupied molecular orbital (LUMO). Frontier molecular orbital (FMO) analysis, performed using the same computational parameters, enabled precise calculation of the HOMO–LUMO energy gap. A comprehensive set of molecular descriptors, derived from the calculated orbital parameters, was systematically evaluated. The resulting data, reflecting the electronic structure and reactivity trends of the studied ligands, are graphically illustrated in Figure 14.

Mulliken charge distribution is a method used in computational chemistry to determine the partial atomic charges within a molecule. It is based on the electron density calculated using quantum mechanical methods. This approach originates from Mulliken's population analysis, which takes into account the distribution of electrons across molecular orbitals and basic functions [10,14,41].

The introductory section discusses the fundamental features and interpretive value of Mulliken charges. The positive charges within a molecule indicate regions of electron deficiency, or electrophilic behavior, whereas negative charges denote electron-rich regions, or nucleophilic behavior [42]. This information provides valuable insight into the chemical reactivity of a molecule. Analysis of the Mulliken charge distribution reveals that substitution at the functional group 4 of the aroylhydrazone derivatives in the ligand series results in noticeable variations in electronic properties (Figure 15).

Molecular docking of the Aroyl Hydrazones

In the molecular docking analysis of the H_2L^1–1U1Z complex, the most favorable binding conformation was identified based on key interactions within the active site, exhibiting the highest binding affinity with a docking score of –11.6255 kcal/mol. Electrostatic Van der Waals interactions were observed between VAL530, PRO529, PHE526, ILE492, ILE486, ILE349, PHE374, GLN354, and TYR372 with the H_2L^1 molecule. Specifically, H_2L^1 as a ligand, with its carbon and alkyl groups, interacts with the amino acid fragments VAL490 and ALA353 of the protein, forming hydrophobic π-alkyl effects with the aromatic ring. PHE481 and TYR373 interact with the furan ring, forming a π-π T-shaped interaction, while LEU371 interacts with the furan ring via a π-sigma effect. Additionally, GLU350 forms a π-anion interaction with the aromatic ring. Notably, the oxygen of HIS480, the fluorines of PRO488, and GLY489 participate in hydrogen bond interactions with the H_2L^1 molecule (Figure 16).

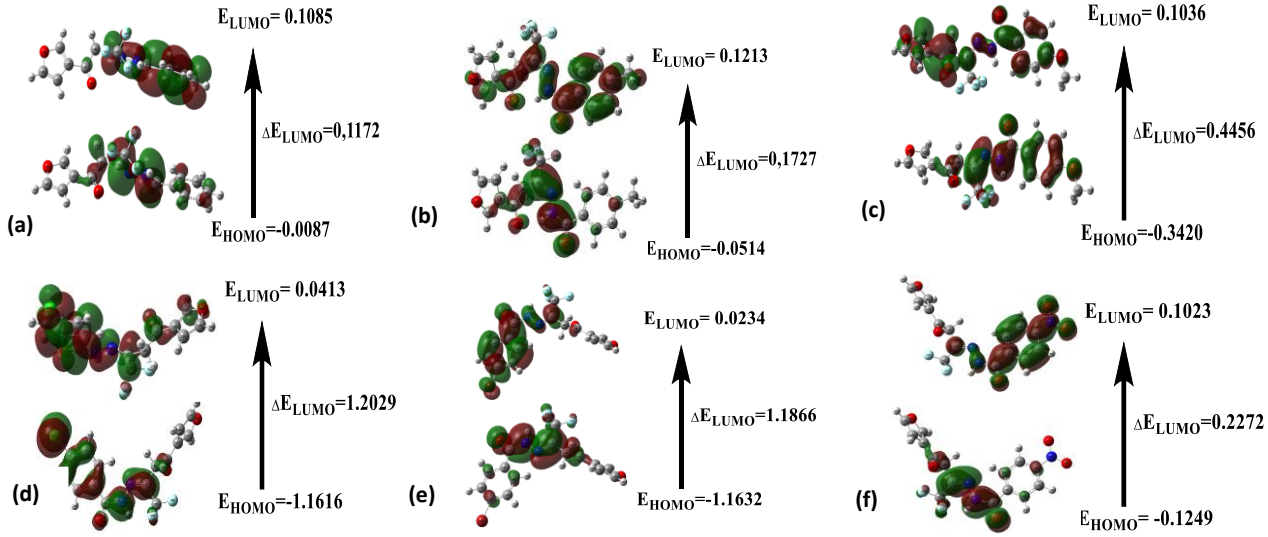

Figure 14. Frontier molecular orbitals HOMO and LUMO energy level: a) H_2L^1, b) H_2L^2, c) H_2L^3, d) H_2L^1, e) H_2L^2, and f) H_2L^3

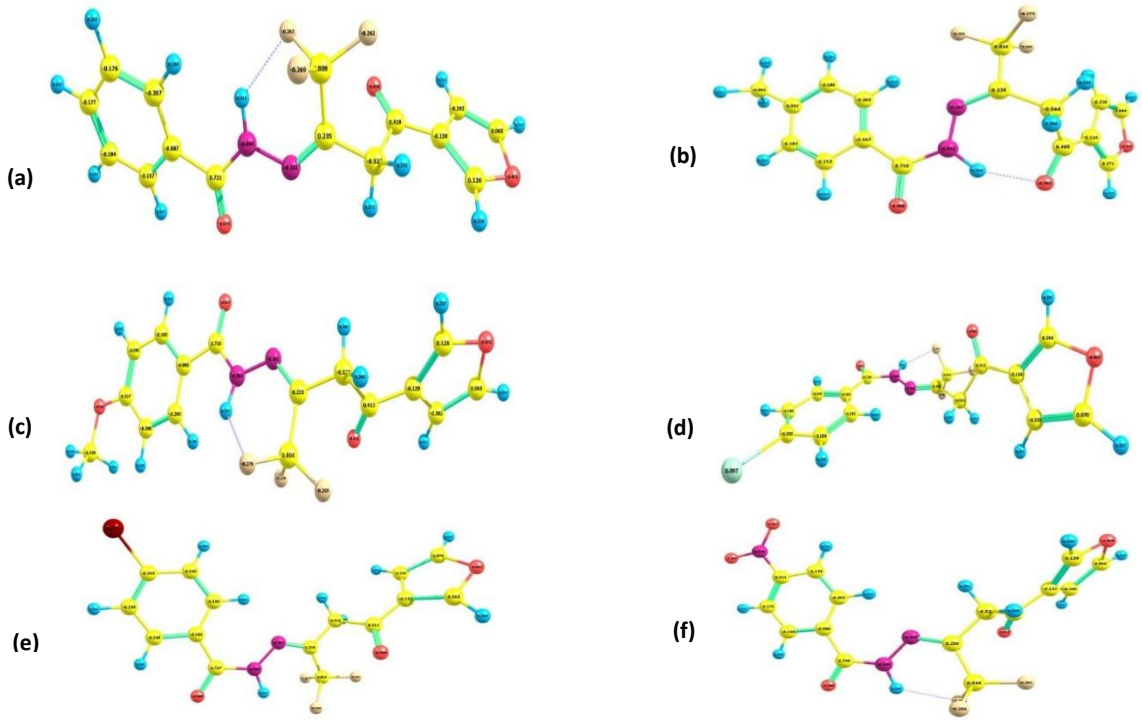

Figure 15. The mulliken charge distribution on the atoms was analyzed for all compounds: a) H_2L^1, b) H_2L^2, c) H_2L^3, d) H_2L^1, e) H_2L^2, and f) H_2L^3

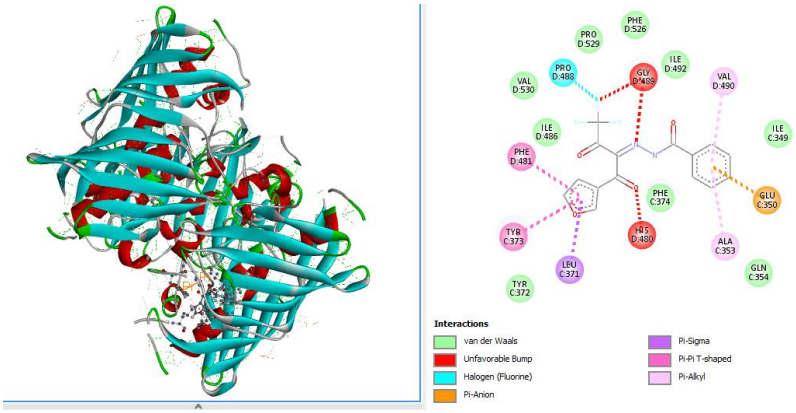

Figure 16. Results of molecular docking of the H_2L^1 molecule

Based on the obtained molecular docking data, it can be concluded that the molecule benzoyl hydrazone 4,4,4-trifluoro-1-(3-furanyl)-1,3-butanedione plays a qualitative role against the bacterium *P. aeruginosa*. Hydrazone derivatives have attracted considerable attention due to their versatile coordination behavior and diverse biological properties. The presence of both azomethine (–CH=N–) and carbonyl (C=O) groups allows these molecules to act as efficient bidentate or tridentate ligands in coordination chemistry, forming stable complexes with transition metals that exhibit interesting catalytic and magnetic properties. Moreover, numerous studies have demonstrated that hydrazones and their metal complexes possess significant medicinal potential, including antimicrobial, anticancer, antioxidant, and anti-inflammatory activities.

Therefore, the synthesized 4,4,4-trifluoro-1-(3-furanyl)-1,3-butanedione -based hydrazones may serve as promising candidates for further exploration in medicinal and coordination chemistry, particularly in designing new biologically active metal complexes [43-45].

Conclusion

In this study, the synthesis of aroyl hydrazones derived from 4,4,4-trifluoro-1-(3-furanyl)-1,3-butanedione was successfully conducted. Structural characterization was performed using IR and NMR spectroscopy, confirming the formation of the target hydrazone derivatives. The vibrational spectra provided clear evidence of key functional groups, while NMR analysis further supported the structural integrity of the synthesized compounds. In addition, DFT calculations were employed to complement the experimental data, providing a deeper understanding of the electronic structure and molecular properties of the synthesized hydrazones. Theoretical results were found to be in good agreement with the experimental findings, supporting the proposed structural features and vibrational assignments. Overall, this work contributes to the expanding body of knowledge on aroyl hydrazones and their spectroscopic characteristics, paving the way for further investigations into their potential applications in medicinal and materials sciences. The studied hydrazones demonstrate promising potential for continued exploration in coordination chemistry and biological applications.

Acknowledgement

The authors are sincerely grateful to the Institute of the Chemistry of Plant Substances named Acad. S. Yu.Yunusov of the Academy of Sciences of the Republic of Uzbekistan for support of this work.

Disclosure Statement

No potential conflict of interest was reported by the authors.

ORCID

Maftuna Jo'rayevna Ruzieva:
https://orcid.org/0000-0003-0234-5929
Murod Amonovich Tursunov:
https://orcid.org/0000-0001-6451-7277
Dana Sapargalievna Belgibayeva:
https://orcid.org/0000-0002-4225-600X
Bakhtiyor Shukurulloyevich Ganiev:
https://orcid.org/0000-0001-8151-1088
Savriyeva Qahramon Qizi Nigina:
https://orcid.org/0000-0003-4600-7868

References

[1] de Gonzalo, G., Alcántara, A.R. Recent developments in the synthesis of β-diketones. *Pharmaceuticals*, **2021**, 14(10), 1043.
[2] Volpi, G., Zago, S., Rabezzana, R., Diana, E., Priola, E., Garino, C., Gobetto, R. *N*-based polydentate ligands and corresponding Zn(II) complexes: A structural and spectroscopic study. *Inorganics*, **2023**, 11(11), 435.
[3] Romanov, D., Vasil'ev, N., Lyamin, A., Ivanovskaya, N., Osinb, N. Synthesis of fluorine-containing tetraketones and diketo esters and luminescence-spectral properties of their complexes with lanthanide ions. *Russian Chemical Bulletin*, **2006**, 55(2), 276–280.
[4] Sumran, G., Jain, N., Kumar, P., Aggarwal, R. Trifluoromethyl-β-dicarbonyls as versatile synthons in synthesis of heterocycles. *Chemistry–A European Journal*, **2024**, 30(11), e202303599.
[5] Fustero, S., Simón-Fuentes, A., Delgado, O., Román, R. Fluorinated pyrazoles and indazoles. *Fluorine in Heterocyclic Chemistry Volume 1: 5-Membered Heterocycles and Macrocycles*, **2014**, 279–321.
[6] Singh, S.P., Kumar, D., Batra, H., Naithani, R., Rozas, I., Elguero, J. The reaction between hydrazines and β-dicarbonyl compounds: Proposal for a mechanism. *Canadian Journal of Chemistry*, **2000**, 78(8), 1109–1120.
[7] Saloutin, V.I., Edilova, Y.O., Kudyakova, Y.S., Burgart, Y.V., Bazhin, D.N. Heterometallic molecular architectures based on fluorinated β-diketone ligands. *Molecules*, **2022**, 27(22), 7894.

[8] Skopenko, V.V., Amirkhanov, V.M., Sliva, T.Y., Vasilchenko, I.S., Anpilova, E.L., Garnovskii, A.D. Various types of metal complexes based on chelating *β*-diketones and their structural analogues. *Russian Chemical Reviews*, **2004**, 73(8), 737–752.

[9] Tayyari, S.F., Nekoei, A.-R., Rahemi, H. Conformation, structure, intramolecular hydrogen bonding, and vibrational assignment of 4, 4, 4-trifluoro-1-(2-furyl)-1, 3-butanedione. *Journal of Molecular Structure*, **2008**, 882(1-3), 153–167.

[10] Darugar, V., Vakili, M., Nekoei, A., Tayyari, S.F., Afzali, R. Tautomerism, molecular structure, intramolecular hydrogen bond, and enol-enol equilibrium of para halo substituted 4, 4, 4-trifluoro-1-phenyl-1, 3-butanedione; experimental and theoretical studies. *Journal of Molecular Structure*, **2017**, 1150, 427–437.

[11] Chauvin, A.S., Gumy, F., Matsubayashi, I., Hasegawa, Y., Bünzli, J.C.G. Fluorinated β-diketones for the extraction of lanthanide ions: Photophysical properties and hydration numbers of their Eu^{III} complexes. *European Journal of Inorganic Chemistry*, **2006**, 2006(2), 473-480.

[12] Varaksina, E.A., Kiskin, M.A., Lyssenko, K.A., Puntus, L.N., Korshunov, V.M., Silva, G.S., Freire, R.O., Taydakov, I.V. Tuning the luminescence efficiency by perfluorination of side chains in Eu^{3+} complexes with *β*-diketones of the thiophene series. *Physical Chemistry Chemical Physics*, **2021**, 23(45), 25748–25760.

[13] Al-Anber, M.A., Daoud, H.M., Rüffer, T., Lang, H. 3D-supermolecular structure and electronic absorption of uranyl *β*-diketone $[UO_2(tfa)_2(L)](L=H_2O, OHCH_2CH_3)$ complex. *Journal of Molecular Structure*, **2011**, 997(1-3), 1–6.

[14] Saleem, M., Rafiq, M., Jeong, Y.K., Cho, D.W., Kim, C.-H., Seo, S.-Y., Choi, C.-S., Hong, S.-K., Lee, K.H. Facile synthesis, crystal structure, DFT calculation and biological activities of 4-(2-fluorophenyl)-3-(3-methoxybenzyl)-1*H*-1, 2, 4-triazol-5 (4*H*)-one (5). *Medicinal Chemistry*, **2018**, 14(5), 451–459.

[15] Avezov, K., Umarov, B., Tursunov, M., Minin, V., Parpiev, N. Copper(II) complexes based on 2-thenoyltrifluoroacetone aroyl hydrazones: Synthesis, spectroscopy, and x-ray diffraction analysis. *Russian Journal of Coordination Chemistry*, **2016**, 42(7), 470–475.

[16] Tursunov, M., Umarov, B., Ergashov, M.Y., Avezov, K. Synthesis and crystal structure of the nickel(II) complex with aroyl hydrazone of ethyl ether of 5, 5-dimethyl-2, 4-dioxohexane acid. *Journal of Structural Chemistry*, **2020**, 61(1), 73–85.

[17] Tafere, D.A., Gebrezgiabher, M., Elemo, F., Atisme, T.B., Ashebr, T.G., Ahmed, I.N. Hydrazones, hydrazones-based coinage metal complexes, and their biological applications. *RSC Advances*, **2025**, 15(8), 6191–6207.

[18] Murugappan, S., Dastari, S., Jungare, K., Barve, N.M., Shankaraiah, N. Hydrazide-hydrazone/hydrazone as enabling linkers in anti-cancer drug discovery: A comprehensive review. *Journal of Molecular Structure*, **2024**, 1307, 138012.

[19] Socea, L.-I., Barbuceanu, S.-F., Pahontu, E.M., Dumitru, A.-C., Nitulescu, G.M., Sfetea, R.C., Apostol, T.-V. Acylhydrazones and their biological activity: A review. *Molecules*, **2022**, 27(24), 8719.

[20] Tayade, K., Yeom, G.-S., Sahoo, S.K., Puschmann, H., Nimse, S.B., Kuwar, A. Exploration of molecular structure, DFT calculations, and antioxidant activity of a hydrazone derivative. *Antioxidants*, **2022**, 11(11), 2138.

[21] Savriyeva, N.Q.Q., Tursunov, M.A., Ganiev, B.S. Novel [5-Hdroxy-3-phenyl-5-(trifluoromethyl)-4,5-dihydro-1*H*-pyrazol-1-yl](phenyl)methanone: Synthesis, characterization and computational analysis. *Advanced Journal of Chemistry, Section A*, **2026**, 9(2), 192-207.

[22] Devi, J., Arora, T. Vanillin derived hydrazone ligands and their transition metal complexes: Synthesis, characterization, biological activity and molecular docking studies. *Journal of Inorganic and Organometallic Polymers and Materials*, **2025**, 1–15.

[23] Filatov, M., Lee, S., Nakata, H., Choi, C.H. Computation of molecular electron affinities using an ensemble density functional theory method. *The Journal of Physical Chemistry A*, **2020**, 124(38), 7795–7804.

[24] Frisch, M.J., Nielsen, A.B. Gaussian 03 programmer's reference. **2003**.

[25] Caricato, M., Frisch, M.J., Hiscocks, J., Frisch, M.J. Gaussian 09: Iops reference. **2009**.

[26] Bitencourt-Ferreira, G., de Azevedo Jr, W.F. Molecular docking simulations with arguslab. *Docking Screens for Drug Discovery*, **2019**, 203–220.

[27] Baroroh, U., Biotek, M., Muscifa, Z.S., Destiarani, W., Rohmatullah, F.G., Yusuf, M. Molecular interaction analysis and visualization of protein-ligand docking using biovia discovery studio visualizer. *Indonesian Journal of Computational Biology (IJCB)*, **2023**, 2(1), 22–30.

[28] Jejurikar, B.L., Rohane, S.H. Drug designing in discovery studio. **2021**, 135-138.

[29] Yang, T., Deng, Z., Wang, K.H., Li, P., Huang, D., Su, Y., Hu, Y. Synthesis of polysubstituted trifluoromethylpyridines from trifluoromethyl-α,β-ynones. *The Journal of Organic Chemistry*, **2020,** 85(2), 924–933.

[30] Joule, J.A. Heterocyclic chemistry. *Book*, **2020**, 720.

[31] Ferrari, M., Mottola, L., Quaresima, V. Principles, techniques, and limitations of near infrared

spectroscopy. *Canadian Journal of Applied Physiology*, **2004**, 29(4), 463–487.
[32] Avezov, K.G., Umarov, B.B., Ganiev, B.S., Zaynieva, R.B., Kholikova, G.K., Panova, E.V., Safin, D.A. Novel 2-benzoyl-3-hydroxy-3-(trifluoromethyl)-3, 3a,4,5,6,7-hexahydro-2*H*-indazole: Synthesis, characterization and computational analysis. *Journal of Molecular Structure*, **2025**, 1343, 142740.
[33] Bratenko, M., Sidorchuk, I., Khalaturnik, M., Vovk, M. Synthesis and antimicrobial activity of new azomethines synthesized from 4-formyl-1-phenyl-3-aryl (heteryl) pyrazoles. *Pharmaceutical Chemistry Journal*, **1999**, 33(2), 81–83.
[34] Sloop, J.C., Churley, M., Guzman, A., Moseley, S., Stalker, S., Weyand, J., Yi, J. Synthesis and reactivity of fluorinated cyclic ketones: Initial findings. *American Journal of Organic Chemistry*, **2014**, 4(1), 1–10.
[35] Günther, H. NMR spectroscopy: basic principles, concepts and applications in chemistry. Book, **2013**, 630.
[36] Abduraxmonov, S., Tursunov, M., Umarov, B., Ergashov, M.Y., Avezov, K. Research on nickel(II) complexes with aroyl hydrazones of 5,5-dimethyl-2,4-dioxohexanoic acid ethyl ester. *Moscow University Chemistry Bulletin*, **2020**, 75(6), 395–401.
[37] Ganiev, B., Mardonov, U., Kholikova, G. Molecular structure, HOMO-LUMO, MEP-–analysis of triazine compounds using DFT (B3LYP) calculations. *Materials Today: Proceedings*, **2023**.
[38] Santhy, K., Sweetlin, M.D., Muthu, S., Kuruvilla, T.K., Abraham, C.S. Structure, spectroscopic study and DFT calculations of 2, 6 bis (tri fluro methyl) benzoic acid. *Journal of Molecular Structure*, **2019**, 1177, 401–417.
[39] Hauge, E.S. Extrapolating the Electric Dipole Moment. Master's thesis, **2021**,132.
[40] Zhao, L., Pan, S., Frenking, G. The nature of the polar covalent bond. *The Journal of Chemical Physics*, **2022**, 157(3), 034105.
[41] Demircioğlu, Z., Kaştaş, Ç.A., Büyükgüngör, O. Theoretical analysis (NBO, NPA, mulliken population method) and molecular orbital studies (hardness, chemical potential, electrophilicity and fukui function analysis) of (*E*)-2-((4-hydroxy-2-methylphenylimino) methyl)-3-methoxyphenol. *Journal of Molecular Structure*, **2015**, 1091, 183–195.
[42] Gomez-Jeria, J.S. An empirical way to correct some drawbacks of mulliken population analysis. *Journal of the Chilean Chemical Society*, **2009**, 54(4), 482–485.
[43] Liu, R., Cui, J., Ding, T., Liu, Y., Liang, H. Research progress on the biological activities of metal complexes bearing polycyclic aromatic hydrazones. *Molecules*, **2022**, 27(23), 8393.
[44] Ribeiro, N., Correia, I. A review of hydrazide-hydrazone metal complexes' antitumor potential. *Frontiers in Chemical Biology*, **2024**, 3, 1398873.
[45] Shakdofa, M.M., Shtaiwi, M.H., Morsy, N., Abdel-rassel, T.M. Metal complexes of hydrazones and their biological, analytical and catalytic applications: A review. *Main Group Chemistry*, **2014**, 13(3), 187–218.

HOW TO CITE THIS ARTICLE

M.J. Ruzieva, M.A. Tursunov, D.S. Belgibayeva, S.A. Karomatov, B.S. Ganiev, S.Q.Q. Nigina. Synthesis, IR and NMR–Spectroscopic, DFT Study of Aroyl Hydrazones 4,4,4-Trifluoro-1-(3-Furanyl)-1,3-Butanedione. *Adv. J. Chem. A*, 2026, 9(6), 1031-1047.

DOI: 10.48309/AJCA.2026.549860.1945
URL: https://www.ajchem-a.com/article_238819.html